Cross-section set and chemistry model for the simulation of c-C_4F_8 plasma discharges

G. I. Font,[a] W. L. Morgan,[b] and G. Mennenga
Kinema Research and Software, P.O. Box 1147, Monument, Colorado 80132

(Received 24 September 2001; accepted for publication 13 December 2001)

Great interest exists in c-C_4F_8 (octafluorocyclobutane or perfluorocyclobutane) etching plasma discharges due to their selectivity and potential for decreasing global warming gas emissions. In order to allow computational exploration of the discharge physics, a numerical model for a c-C_4F_8 discharge has been constructed. A set of cross sections has been assembled for electron collisions with c-C_4F_8 based on a combination of *ab initio* calculations, beam measurements, and swarm (i.e., electron transport coefficient) analysis. In addition, a chemical reaction set has been proposed and an axisymmetric numerical model has been used to test the cross section and chemical reaction set against experiments. Results show that measured trends are reproduced and absolute values are well represented. A mechanism is suggested for negative atomic fluorine ion (F^-) behavior with respect to power. © *2002 American Institute of Physics.* [DOI: 10.1063/1.1448894]

I. INTRODUCTION

Recently, much study has been devoted to exploring the etching performance of c-C_4F_8 because of its good selectivity of SiO_2 over Si[1,2] and its potential for lowering global warming gas emissions.[3,4] In an effort to understand the plasma composition, species and ion densities have been measured by a variety of methods.[1,5–9] Separate studies have concentrated on understanding the surface processes.[10–13] Comprehensive measurements of ion and neutral densities have not been taken on the same system under equal plasma conditions, however, leaving a fractionated picture of the state of the plasma. A great need, therefore, exists for complete measurements or for a model that can describe the entire plasma state.

Some work has been done to simulate c-C_4F_8 discharges. Ho *et al.*[14] conducted zero-dimensional simulations of c-C_4F_8 plasmas while Kazumi and Tago[15] conducted one-dimensional simulations. These models began to give a complete picture of the plasma state and its behavior. They were, however, of limited applicability to manufacturing processes due to the large gradients present in process reactors which could not be captured in the zero-dimensional (0D) or one-dimensional (1D) models. In order to facilitate understanding of the relationship between the plasma constituents and the results measured on wafers a multidimensional model of a c-C_4F_8 discharge is necessary. This model should be based on as much experimentally measured reaction data as possible. This is not often easy since cross-section measurements (needed for reaction probabilities) drawn from disparate sources are often inconsistent with each other.[16]

In this work, we present a c-C_4F_8 plasma discharge chemistry model. Cross section and rate data has been collected or computed and verified to be consistent with each other and swarm experiments. Elastic, ionization, attachment, and dissociation cross sections are presented as well as integrated Arrhenius type rate expressions. A chemical reaction model is also presented and the combined set is compared with experiments to ascertain its accuracy.

Section II details the chemical reaction model which has been created from published literature, new measurements, swarm analysis, and *ab initio* calculations. Section III describes the two-dimensional numerical model. Comparison of computational results and experiments are presented in Secs. IV and V.

II. ELECTRON COLLISION CROSS SECTIONS AND PLASMA CHEMISTRY

A. c-C_4F_8 cross sections

A set of cross sections has been assembled for electron collisions with c-C_4F_8 based on a combination of *ab initio* calculations, beam measurements, and swarm (i.e., electron transport coefficient) analysis. Novak and Frechette[17] assembled a cross-section set using swarm analysis and the measurements[18] available in 1988. Improved electron swarm calculations were later performed by Itoh *et al.*[19] Now, much better electron transport data are available.[20–22] Christophorou and Olthoff[23] have recently reviewed all previously published electron collision data for c-C_4F_8.

The elastic and momentum transfer cross sections have been calculated by Winstead and McKoy.[24] They have also calculated excitation cross sections for two electronic states of c-C_4F_8. Sanabia *et al.*[25] and Nishimura[26] have measured the total cross section for scattering of electrons by c-C_4F_8. Jiao *et al.*[27] have measured the dissociative ionization cross sections finding that $C_2F_4^+$ and $C_3F_5^+$ have the largest cross sections.

There have been three measurements of the c-C_4F_8 attachment cross section. Kurepa[28] measured the cross section in 1965 at electron energies between 0.1 and 10 eV using an electron beam and ionization chamber. Spyrou *et al.* [see Ref. 29 and references to previous work contained therein]

[a]Electronic mail: font@kinema.com
[b]Electronic mail: morgan@kinema.com

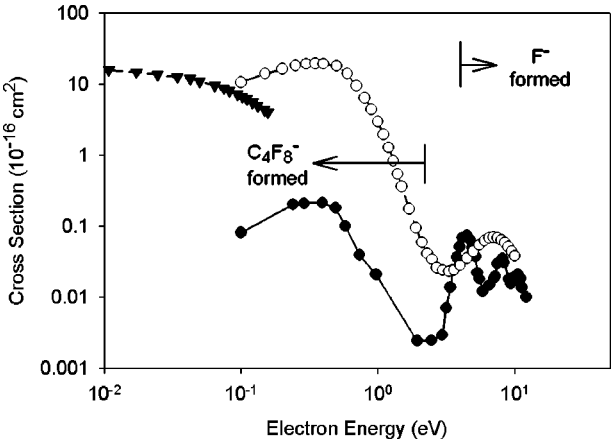

FIG. 1. Electron attachment to c-C_4F_8. Triangles, Ref. 30; open circles, Ref. 29; and filled circles, Ref. 28.

have deduced the cross section from high-pressure swarm measurements and time-of-flight mass spectrometry. Chutjian and Alajajian[30] have measured the very low-energy (below 0.1 eV) attachment cross section using threshold photoionization in krypton gas. The various measured attachment cross sections are shown in Fig. 1. There are two primary attachment mechanisms. At energies above about 1 eV, the dominant process is dissociative attachment forming F^-. At lower energies, c-C_4F_8 attaches forming $C_4F_8^-$. Measurements of the lifetime of $C_4F_8^-$ against autodetachment range from 10 to 500 μs,[23] where the lifetime of the complex may depend upon the kinetic energy of the attaching electron. Because of the finite lifetime, at low-electron energies the cross section or attachment rate measured in a given apparatus may depend on the collisional mean free path of the negative ion relative to the dimensions of the apparatus and on the mean time between collisions with another gas molecule compared with the autodetachment lifetime.

Because the measured cross section or rate coefficient can depend on the size of the apparatus and on the pressure, there tend to be significant differences between the apparent cross sections that are measured. This will be discussed further below.

1. Swarm analysis

The electron drift velocity calculated from the solution $f_0(\epsilon)$ of Boltzmann's equation is defined as

$$V_d = \langle v_z \rangle = -\tfrac{1}{3}(2e/m)^{1/2}(E/N) \times \int [df_0(\epsilon, E/N)/d\epsilon]\epsilon d\epsilon/\sigma_m, \quad (1)$$

where

ϵ=electron energy

e=electron charge

m=electron mass

E/N=electric field divided by gas number density ($\mathbf{E} = E\mathbf{z}$)

f_0=electron energy distribution function

σ_m=momentum transfer cross section.

The *momentum transfer cross section* $\sigma_m(\epsilon)$ is defined by

$$\sigma_m(\epsilon) = 2\pi \int \sigma_e(\epsilon, \theta)(1-\cos\theta)\sin\theta d\theta, \quad (2)$$

where $\sigma_e(\epsilon, \theta)$ is the differential cross section for elastic scattering. The momentum transfer cross section is also known in transport theory as the diffusion cross section. The ionization rate coefficient is defined as

$$k_i = (2e/m)^{1/2} \int \sigma_i(\epsilon) f_0(\epsilon, E/N)\epsilon d\epsilon, \quad (3)$$

where σ_i is the ionization cross section. The ionization coefficient measured in a swarm experiment is

$$\alpha = k_i N/V_d, \quad (4)$$

which is the increase in electron density per centimeter due to ionization as a swarm of electrons drifts against an electric field. This is usually displayed as α/N with units of cm^2.

The connection to microscopic electron collision physics is made explicitly through the cross sections and the electron energy distribution function $f_0(\epsilon)$. The latter is the solution to Boltzmann's equation for electron transport in a plasma. All the microscopic physics implicit in the electron transport or swarm coefficients appear in Boltzmann's equation as dependencies on the electric field; gas, ion, and electron densities; and all elastic and inelastic collision cross sections (see the review by Morgan[16]).

Boltzmann's equation can be solved numerically[16,31] and the numerical solutions can be used in deducing electron collision cross sections from a set of measured electron transport coefficients. We use the two-term spherical harmonic approximation to the solution of Boltzmann's equation.[31] Because we solve for the steady-state electron energy distribution function $f_0(\epsilon)$ by integrating an equation for $df_0(\epsilon, t)/dt$ in time we are able to include the effects of ionization and attachment on $f_0(\epsilon)$. Attachment removes electrons preferentially from parts of $f_0(\epsilon)$ and ionization produces low-energy secondary electrons that tend to increase $f_0(\epsilon)$ at low energies. These processes, of course, can then affect the calculated transport coefficients.

Swarm analyses can be performed in a variety of ways. The most common method, historically, is to postulate a set of cross sections and manipulate their energy dependencies and magnitudes such that transport coefficients computed by solving Boltzmann's equation agree with measured values. Since we have available to us state-of-the-art *ab initio* calculations of the momentum transfer and electronic excitation cross sections and high-quality ionization cross section measurements, we have previously also used the approach of adding some model vibrational excitation cross sections to the set to take into account energy loss at low values of E/N and then adjusting the magnitudes of the cross sections to achieve consistency with measured swarm coefficients. We use the downhill simplex and simulated annealing algorithms[32,33] in our swarm analysis[34,35] in order to adjust the magnitudes and shapes of the cross sections to achieve a minimum in the root-mean-square (rms) difference between the sets of measured and computed transport coefficients.

We have used the Born approximation forms[36] for our model vibrational excitation cross sections. If $\Delta\epsilon$ is the vi-

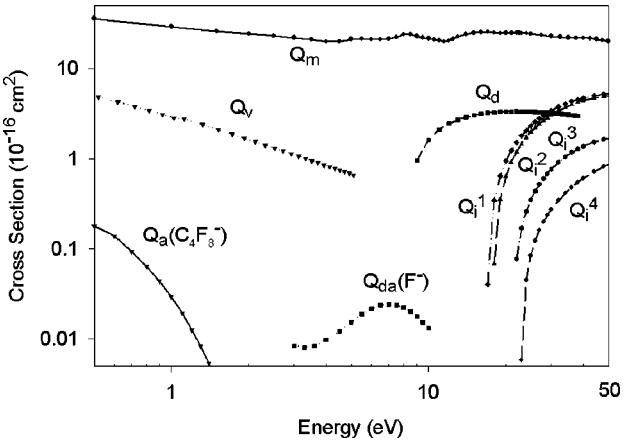

FIG. 2. c-C_4F_8 electron collision cross sections. Momentum transfer, Q_m; Vibrational excitation, Q_v; Attachment forming $C_4F_8^-$ and F^-; dissociation, Q_d; Ionization forming $C_2F_4^+$, Q_i^1; $C_3F_5^+$, Q_i^2; CF_3^+, Q_i^3; and CF_2^+, Q_i^4.

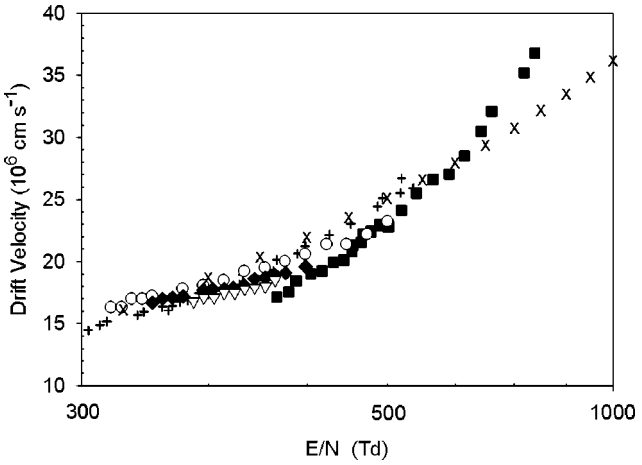

FIG. 3. Measured and calculated drift velocities for electrons in c-C_4F_8. The inverted triangles, diamonds, and open circles are from Ref. 20 at 2–7.5 Torr, 1 Torr, and 0.6 Torr, respectively; the squares are from Ref. 22 (see Ref. 23); the cross hairs are from Ref. 18; and the x's are our calculations.

brational excitation energy in eV and ϵ is the electron impact energy the energy dependence of the Born approximation cross section for excitation is

$$\sigma_V^B = 3.7\times 10^{-15}/(\Delta\epsilon x)\ln[(x^{1/2}+(x-1)^{1/2})/|x^{1/2}-(x-1)^{1/2}|], \quad (5)$$

where $x=\epsilon/\Delta\epsilon$. This has been normalized such that the $\sigma_V^B = 1\times 10^{-16}\,\mathrm{cm}^2$ at its peak. Because we adjust the magnitudes of the vibrational excitation cross sections to give agreement with the measured swarm data, it is only the energy dependence of the Born cross section that is of interest to us. We have used in our analysis a single vibrational level for c-C_4F_8 having an energy of 0.12 eV.

2. Recommended cross-section set

We have used here the same approach used in our previous work on CHF_3[37] and C_2F_4[38] for estimating the electron impact dissociation cross section. If we fix the ionization cross sections to the measured values we can vary the momentum transfer and dissociation cross sections in order to obtain a good fit to the measured drift velocity and ionization and attachment coefficients. In these fits we gave more weight to the most recently measured data. For the c-C_4F_8 analysis, the excitation cross sections calculated by Winstead and McKoy[24] were not sufficient so we used a model cross section of the form

$$\sigma_d(\epsilon) = \sigma_d^0 \ln(\epsilon/\Delta\epsilon)/(\epsilon/\Delta\epsilon), \quad (6)$$

where $\Delta\epsilon$ is the excitation threshold energy of 8 eV. Because the calculated swarm coefficients agree very well with the measurements, we are confident that our model cross section is a reasonable representation of a composite dissociation cross section.

Our final cross section set is shown in Fig. 2. The agreement with the measured swarm coefficients is shown in Figs. 3 and 4. Our momentum transfer cross section is 0.9 times that calculated by Winstead and McKoy. In order to obtain agreement with the measured electron growth coefficient we multiplied the attachment cross section for the formation of $C_4F_8^-$ from Spyrou *et al.*[29] by 10^{-2} and that for formation of F^- by 0.35. Although we began the analysis using the attachment cross sections of Spyrou *et al.*[29] our resulting cross sections are very close to those measured by Kurepa.[28] Our analysis is insensitive to the value of the cross section at very low energies such as in the measurements of Chutjian and Alajajian.[30]

All the swarm measurements in pure c-C_4F_8[18,20,22] were performed at gas pressures of ~1 Torr. De Urquijo and Basurto[20] varied the c-C_4F_8 pressure and found measureable changes in the transport coefficients. Their measured attachment coefficient was found to increase substantially with increasing pressure. These effects are, presumably, due to the effects of auto detachment of $C_4F_8^-$ on the swarm measurements. Of the two attachment cross sections shown in Fig. 1 that have been measured or deduced at energies greater than 0.1 eV, that of Spyrou *et al.*[29] was measured at relatively high pressure and that of Kurepa[28] was measured at ex-

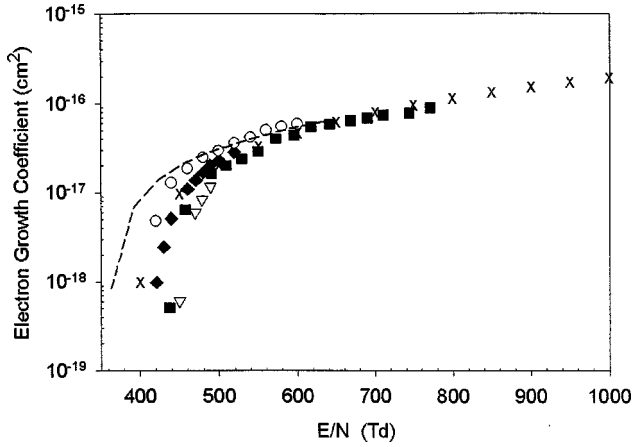

FIG. 4. Measured and calculated electron growth coefficients, α/N−η/N, for electrons in c-C_4F_8. The inverted triangles, diamonds, and open circles are from Ref. 20 at 2–7.5 Torr, 1 Torr, and 0.6 Torr, respectively; the squares are from Ref. 22 (see Ref. 23); the dashed line is from Ref. 18; and the x's are our calculations.

TABLE I. c-C_4F_8 dissociation channels having thresholds of less than 5 eV.

Dissociation products	Energy (eV)
$CF{\equiv}C-CF_3+CF_4$	0.69
$CF_2-C-CF_2+CF_4$	0.86
$C_2F_6+C_2F_2$	2.23
$1-C_3F_6+CF_2$	2.41
$C_2F_4+C_2F_4$	2.42
$CF_2{=}C-CF_3+CF_3$	3.80
$CF_2-CF{=}CF_2+CF_3$	4.09
$CF_3-CF{=}CF+CF_3$	4.13
$C_2F_2+CF_4+CF_2$	4.59
$C_2F_5+C_2F_3$	4.65
$CF_3-CF-CF_3+CF$	4.79
$c-C_4F_7+F$	4.88

TABLE II. C_2F_4 dissociation channels and energetics.

Dissociation products	Energy (eV)
CF_2+CF_2	3.06
CF_3+CF	4.52
C_2F_3+F	5.19
$C_2F_2+F_2$	7.09
C_2F_2+F+F	8.13
CF_2+CF+F	8.13
CF_3+C+F	9.79

tremely low (sub-milli Torr) pressures. The former is more indicative of the total number of $C_4F_8^-$ formed whereas the latter may be much smaller due to the decay of many of the negative ions.

Our modifications of the attachment cross sections reflect the low-pressure effects in the swarm measurements and are probably more appropriate to the plasma chemistry found in low-pressure processing reactors. We are exploring further the effects of formation and destruction of the parent negative ion on swarm measurements using three dimensional Monte Carlo simulations of swarm measurements.

A dissociation cross section has been measured by Toyoda *et al.*[39] that is much smaller than that shown in Fig. 2. Typically, however, the dissociation cross sections measured by this group are smaller than those deduced from swarm analysis or from the total dissociation cross sections measured by others and from cross sections calculated by *ab initio* means. Our cross section does not represent any particular dissociation channel but, rather indicates the approximate magnitude and energy dependence of the total cross section for dissociation into neutral products that c-C_4F_8 must have based on analysis of the ionization coefficient and

TABLE III. Electron impact reactions with c-C_4F_8 and its dissociation products.

Reaction	α	β	γ
$e+C_4F_8 \rightarrow C_4F_8(v)+e$	3.39×10^{-8}	−1.093	0.6346
$e+C_4F_8 \rightarrow 2C_2F_4+e$	9.580×10^{-8}	0.04153	8.572
$e+C_4F_8 \rightarrow C_2F_4^++e$	5.698×10^{-8}	0.4702	17.48
$e+C_4F_8 \rightarrow C_3F_5^++e$	6.655×10^{-8}	0.4095	18.71
$e+C_4F_8 \rightarrow CF_3^++e$	2.688×10^{-8}	0.3794	22.30
$e+C_4F_8 \rightarrow CF_2^++e+e$	4.840×10^{-8}	−.02637	27.03
$e+C_4F_8 \rightarrow C_2F_8^-$	2.960×10^{-11}	−1.328	.2344
$e+C_4F_8 \rightarrow F^-$	2.789×10^{-9}	−1.277	5.392
$e+C_2F_4 \rightarrow e+CF_2+CF_2$	1.315×10^{-8}	0.4118	6.329
$e+C_2F_4 \rightarrow C_2F_4^++e+e$	3.583×10^{-9}	0.6613	11.06
$e+C_2F_4 \rightarrow C_2F_3^++e+e+F$	3.025×10^{-9}	0.8740	16.41
$e+C_2F_4 \rightarrow CF^++e+e+CF_3$	5.874×10^{-9}	0.6188	19.29
$e+CF_3 \rightarrow e+CF_2+F$	6.484×10^{-8}	−0.9578	11.25
$e+CF_3 \rightarrow e+CF_2+F$	7.941×10^{-8}	−0.4517	12.10
$e+CF_3 \rightarrow CF_3^++e+e$	1.356×10^{-9}	0.7963	9.057
$e+CF_3 \rightarrow e+e+CF_2^++F$	7.020×10^{-9}	0.4297	16.28
$e+CF_3 \rightarrow e+e+CF^++F_2$	4.148×10^{-8}	−0.3413	24.28
$e+CF_3 \rightarrow F^-+CF_2$	1.000×10^{-10}	0	0
$e+CF_2 \rightarrow e+CF+F$	3.867×10^{-8}	−0.4250	6.320
$e+CF_2 \rightarrow e+CF+F$	3.324×10^{-8}	−0.5052	2.582
$e+CF_2 \rightarrow e+CF+F$	1.158×10^{-8}	−0.3803	14.35
$e+CF_2 \rightarrow CF_2^++e+e$	1.103×10^{-8}	0.3929	11.37
$e+CF_2 \rightarrow e+e+CF^++F$	5.434×10^{-9}	0.5608	14.29
$e+CF_2 \rightarrow F^-+CF$	1.000×10^{-10}	0	0
$e+CF \rightarrow e+C+F$	2.621×10^{-8}	−0.5701	8.033
$e+CF \rightarrow e+C+F$	1.986×10^{-8}	−0.5229	8.426
$e+CF \rightarrow e+C+F$	4.514×10^{-8}	−0.1098	8.941
$e+CF \rightarrow CF^++e+e$	5.480×10^{-9}	0.5561	9.723
$e+CF \rightarrow F^-+C$	1.000×10^{-10}	0	0
$e+F \rightarrow F^++e+e$	2.397×10^{-9}	0.8476	16.78
$e+F_2 \rightarrow e+F+F$	1.080×10^{-8}	−0.2955	4.464
$e+F_2 \rightarrow F^-+F$	5.768×10^{-9}	−1.465	0.5389
$e+F_2 \rightarrow F_2^++e+e$	2.886×10^{-9}	0.8809	15.91
$e+C \rightarrow C^++e+e$	1.916×10^{-8}	0.4898	12.09

the ionization cross section. Our proposed dissociation cross section has been found to be consistent with measurements of c-C_4F_8 dissociation in a low pressure, inductively coupled reactor.[40]

B. Cross sections and rate coefficients for dissociation products

Because c-C_4F_8 is easily dissociated by electron impact and many of its dissociation products are themselves readily dissociated, we desire to have electron impact cross sections for the various product molecules. In our modeling we have assumed c-C_4F_8 is dissociated into two C_2F_4 molecules. The dissociation energetics of c-C_4F_8 have been calculated by Winstead and McKoy.[41] Dissociation channels having thresholds of less than 5 eV are listed in Table I. Clearly the dissociation kinetics of c-C_4F_8 in the plasma environment may be very complicated. Our choice of products is only one of many possibilities but, since it is well known that thermal dissociation of c-C_4F_8 produces copious quantities of C_2F_4, it is not an unreasonable choice.

Yoshida *et al.*[38] have recently constructed a cross section set for C_2F_4 using *ab initio* calculations,[42] ionization cross-section measurements,[43] and swarm analyses. This cross section set, of which an important component is the C_2F_4 dissociation cross section, has been incorporated into our plasma chemistry model. The computed dissociation energetics for C_2F_4 are listed in Table II.[41] The most likely product channels are $2CF_2$ or CF_3+CF. We have made use of the first channel in our modeling.

We also have available to us cross section sets for CF_3, CF_2, and CF. The elastic and excitation cross sections have been computed by Winstead and McKoy[41] and the dissociative ionization cross sections have been measured by Tarnovsky *et al.*[44]

We have computed the rate coefficients for electron collisions with c-C_4F_8, C_2F_4, CF_3, CF_2, and CF and fit them to the Arrhenius form

$$k(T_e)=\alpha T_e^{\beta}\exp[-\gamma/T_e]. \tag{7}$$

The results are tabulated in Table III and graphed in Fig. 5.

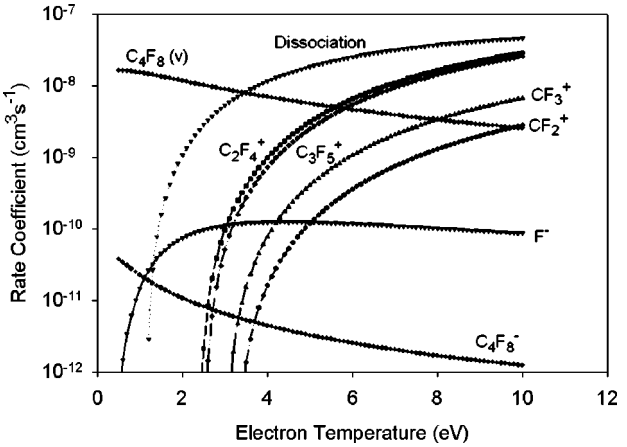

FIG. 5. Rate coefficients for electrons collisions with c-C_4F_8 forming various products. The curve labeled ''Dissociation'' represents the total rate for neutral dissociation.

The reactions that comprise our gas-phase plasma chemistry model are listed in Table IV. Because we are modeling low pressure gas discharges we have included in the heavy particle chemistry model only ion–molecule and ion–ion reactions. The rate coefficients for ion–molecule collisions have been computed using Langevin's theory for nonpolar species or the adiabatic invariance results of Bates and Morgan[45,46] for polar molecules. The rate coefficients for bimolecular ionic recombination have been computed using the formulation of Hickman.[47,48]

III. NUMERICAL MODEL

In order to verify the validity of the model detailed above, simulations were conducted of a c-C_4F_8 discharge using the commercial code PLASMATOR™. This section will briefly lay out the details of numerical model.

PLASMATOR™ uses a fluid model for all species and assumes an axisymmetric geometry (r,z). The plasma model was originally developed at the Lawrence Livermore National Laboratory. Details concerning treatment of ions, electrons, and electromagnetics, can be found in Refs. 49–51. The plasma model has been augmented with general gas-phase and surface chemistry models and the capability to solve the neutral continuity and energy equations. The neutral species equations are solved assuming diffusion dominated transport

$$\frac{\partial n_i}{\partial t}=-\nabla\cdot(D_{ij}\nabla n_i)+R_i, \tag{8}$$

TABLE IV. Ion–molecule and ion–ion reactions in c-C_4F_8 plasma chemistry.

Reaction	Rate coefficient ($cm^3\,s^{-1}$)
$CF_2^+ + C_4F_8 \rightarrow C_3F_5^+ + C_2F_4 + F$	2.10×10^{-11}
$CF_2^+ + CF_3 \rightarrow CF_3^+ + CF_2$	1.48×10^{-9}
$CF_2^+ + CF \rightarrow CF_3^+ + C$	2.06×10^{-9}
$CF_2^+ + C \rightarrow CF^+ + CF$	1.04×10^{-9}
$CF^+ + CF_3 \rightarrow CF_3^+ + CF$	1.71×10^{-9}
$C^+ + CF_3 \rightarrow CF_2^+ + CF$	2.48×10^{-9}
$C^+ + CF \rightarrow CF^+ + C$	3.18×10^{-9}
$F^+ + CF_3 \rightarrow CF_2^+ + F_2$	2.09×10^{-9}
$F^+ + CF_2 \rightarrow CF^+ + F_2$	2.28×10^{-9}
$F^+ + CF \rightarrow C^+ + F_2$	2.71×10^{-9}
$F^+ + C \rightarrow C^+ + F$	1.17×10^{-9}
$F^+ + F_2 \rightarrow F_2^+ + F$	7.94×10^{-10}
$F_2^+ + CF_3 \rightarrow CF_3^+ + F + F$	1.60×10^{-9}
$F_2^+ + CF_2 \rightarrow CF_3^+ + F$	1.79×10^{-9}
$F_2^+ + CF \rightarrow CF_2^+ + F$	2.18×10^{-9}
$F_2^+ + C \rightarrow CF^+ + F$	1.04×10^{-9}
$C_2F_4^+ + F^- \rightarrow CF + CF_2 + F_2$	8.20×10^{-8}
$C_3F_5^+ + F^- \rightarrow C_2F_4 + CF_2$	8.00×10^{-8}
$CF_3^+ + F^- \rightarrow CF_2 + F_2$	8.70×10^{-8}
$CF_2^+ + F^- \rightarrow CF + F_2$	9.10×10^{-8}
$CF^+ + F^- \rightarrow CF + F$	9.80×10^{-8}
$C^+ + F^- \rightarrow C + F$	1.20×10^{-7}
$F^+ + F^- \rightarrow F + F$	1.10×10^{-7}
$F_2^+ + F^- \rightarrow F + F_2$	9.40×10^{-8}

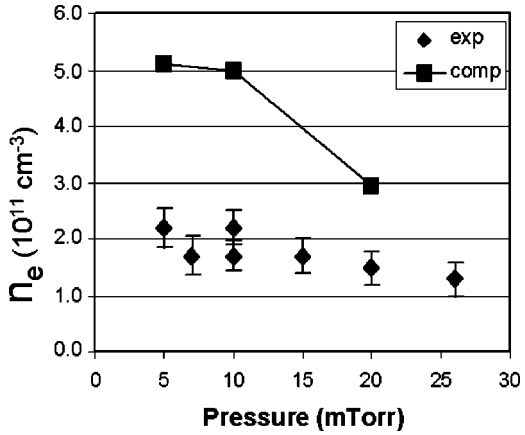

FIG. 6. Electron density vs discharge pressure for the experiments (Ref. 9) and computations. Conditions: 10 sccm C_4F_8; 200 W ICP.

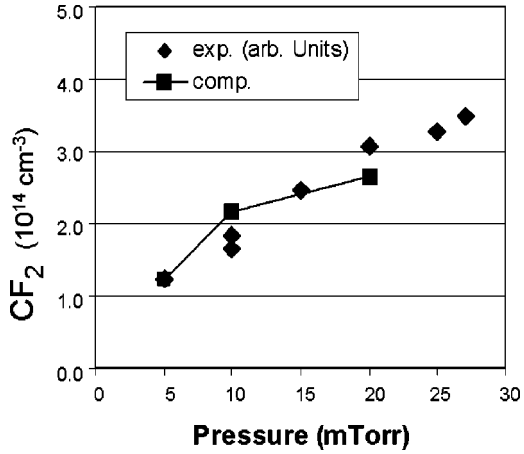

FIG. 8. Computational CF_2 density and experimental (Ref. 9) CF_2 signal vs pressure. Conditions: 10 sccm C_4F_8; 200 W ICP.

$$\frac{\partial}{\partial t}(n_i M_i C_V T) = \nabla \cdot (k_T \nabla T) + M_i C_V \nabla \cdot (D_{ij} T \nabla n_i) + S_i . \tag{9}$$

This assumption is good at low pressures (100 mTorr and below) but, in practice, gives reasonable results at Torr type pressures. In (8) and (9) above, D_{ij} is the diffusion coefficient, R_i is the chemical species source term, M_i is the species mass, C_v is the specific heat, T is the temperature, k_T is the thermal conductivity coefficient, and S_i is the heating source term due to electron inelastic collisions. In the future, the limit to the present approximations will be explored by including the full neutral momentum equation.

IV. VALIDATION OF NUMERICAL AND CHEMISTRY MODEL

Using the model detailed above, simulations were conducted of a c-C_4F_8 discharge in a standard GEC cell. For the simulations, the inductively coupled power was set to 200–350 W. The pressure was varied from 5 to 20 mTorr and the flow rate was set to 10 sccm of c-C_4F_8.

Figure 6 shows the experimental electron density measurements from Hebner[9] plotted against the computational results. The pressure is varied from 5–20 mTorr while the ICP power is held constant at 200 W. The electron density decreases as the pressure increases. The computations capture this behavior, although, they over-predict the electron densities by a factor of 2 at the lowest pressures. This may be related to the formation of $C_4F_8^-$ in the low-pressure plasma chemistry. The electron density decreases with increasing pressure because the electron temperature also decreases leading to diminished ionization. This occurs because the density of the background gas rises with pressure resulting in increased electron energy loss from collisions with the neutral gas. Figure 7 shows the F^- density variation with discharge pressure. The computations do a reasonable job of capturing the F^- density magnitude as well as the behavior. The falling electron density and pressure should result in diminished F^- production with increasing pressure (as shown in the reaction rate of dissociative-attachment below 4 eV in Fig. 5), but because the density of C_4F_8 has tripled when going from 10 to a 30 mTorr discharge, the result is an absolute increase in the F^- density. For the same reason, the absolute amount of CF_2 increases with increasing pressure, even though the rates and the dissociation fraction is actually decreasing. This is clearly shown in Fig. 8. The computations accurately follow the experimentally measured increase in CF_2 signal as the pressure increases. A comparison with ab-

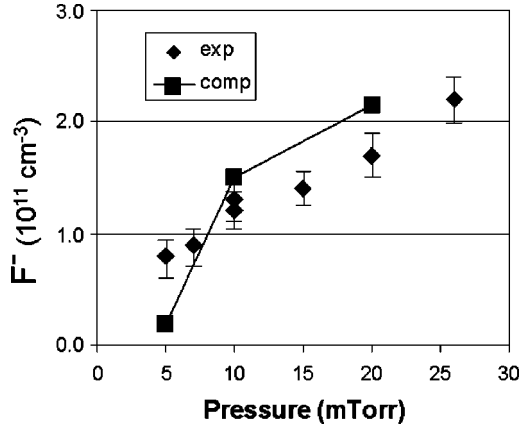

FIG. 7. Negative Fluorine Ion (F^-) density vs pressure for the experiments (Ref. 9) and computations. Conditions: 10 sccm C_4F_8; 200 W ICP.

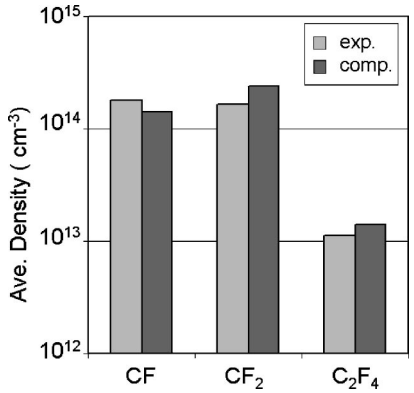

FIG. 9. Absolute average densities of dissociated products, CF, CF_2, and C_2F_4, for the experiments (Ref. 52) and computations vs pressure. Conditions: 10 sccm C_4F_8; 350 W ICP; 15 mTorr.

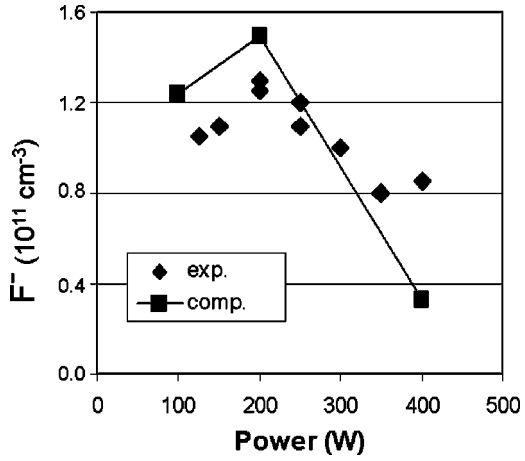

FIG. 10. Negative fluorine ion (F^-) density vs ICP power for the experiments (Ref. 8) and computations. Conditions: 10 sccm C_4F_8; 10 mTorr.

solute density measurements of CF, CF_2, and C_2F_4 from Refs. 52 is presented in Fig. 9. It shows that the chemistry and numerical model do a good job of predicting the absolute amount of dissociation and the relative distribution of some of the dissociated products.

A rather interesting behavior is exhibited by the c-C_4F_8 discharge when the power is varied. When the power is low, the F^- density increases with increasing power. When the power is high, however, the F^- density decreases with increasing power. This is corroborated with experiments[8] and is shown in Fig. 10. The chemistry and numerical model capture this behavior and do a reasonable job of predicting the absolute F^- density. The reason for this is believed to be linked to the C_4F_8 dissociative attachment process. As the power increases, the electron density also increases which leads to enhanced F^- production through dissociative attachment. As the power increases further, the average electron temperature also increases, approximately linearly from 2.3 eV at 100 W to 2.8 eV at 400 W. This would suggest that the F^- production should also increase. However, as shown in Fig. 5, the total dissociation rate is more than an order of magnitude greater than the F^- production rate from dissociative attachment. In addition, the dissociation rate is increasing (in the neighborhood of 2 to 3 eV) in excess of 10 times faster than the F^- production rate. The result is that the small increase in electron temperature raises the dissociation rate to such a great extent, that the amount of C_4F_8 available for dissociative attachment is reduced sufficiently to halt the increase in absolute F^- density.

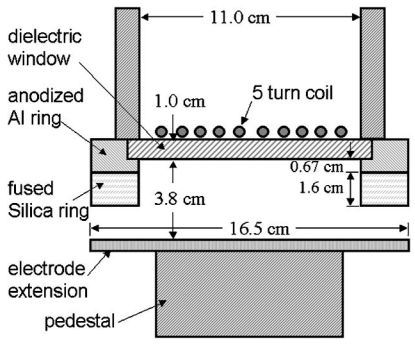

FIG. 11. Gaseous electronics conference (GEC) reference cell configuration.

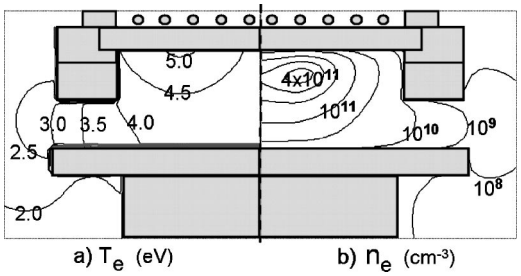

FIG. 12. Electron temperature (a) and electron density (b) contours. Conditions: 10 sccm C_4F_8; 20 mTorr; 200 W ICP.

V. NUMERICAL RESULTS

In this section, the density and temperature contours for a sample GEC ICP discharge are presented. A schematic of the GEC reference cell is shown in Fig. 11. It uses a five-turn coil placed above the discharge region, a fused silica antenna collar, and an extended lower electrode, which remained grounded for the present simulations. The conditions chosen are 10 sccm of c-C_4F_8, 20 mTorr, and 200 W inductively coupled power. Only the part of the computational domain centered on the discharge region will be displayed in the figures.

Figure 12 shows the electron temperature and density contours. The electron temperature reaches 5 eV near the dielectric window [Fig. 12(a)]. The electron density [Fig. 12(b)] peaks at $4.0\times10^{11}\,\mathrm{cm}^{-3}$ in an annulus. The F^- density (not shown) peaks at $9.0\times10^{11}\,\mathrm{cm}^{-3}$ in the same region indicating that the plasma is electronegative with the ion-to-electron ratio being more than 2 to 1. Figure 13 shows the dominant ion density contours. $C_2F_4^+$ has a maximum density of $7.0\times10^{11}\,\mathrm{cm}^{-3}$ [Fig. 13(a)]. The maximum density of the next most populous ion, CF_2^+, is less than one third of the value of the $C_2F_4^+$, as shown in Fig. 13(b). The CF_2^+ density decreases faster with distance from the discharge center than the $C_2F_4^+$ density. Inspection of the reaction rates in the simulation reveals that the $C_2F_4^+$ density decreases at a lower rate because, while the destruction rate is comparable between the two ions, $C_2F_4^+$ has an additional significant creation channel not available to CF_2^+. It is generated through both dissociative ionization from C_4F_8 and direct

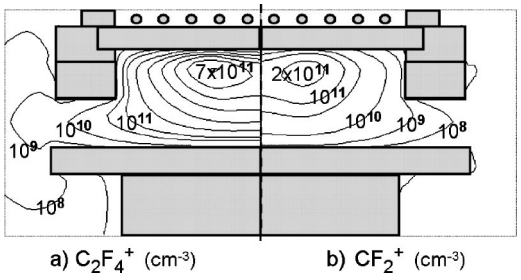

FIG. 13. Dominant ion density contours: (a) $C_2F_4^+$ and (b) CF_2^+. Conditions: 10 sccm C_4F_8; 20 mTorr; 200 W ICP.

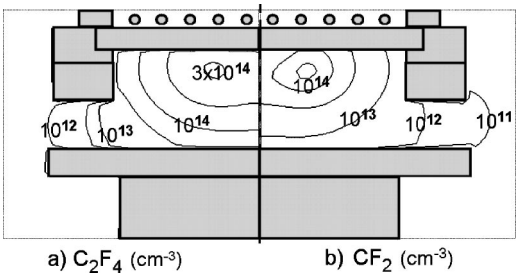

FIG. 14. Dominant dissociated product density contours: (a) C_2F_4 and (b) CF_2. Conditions: 10 sccm C_4F_8; 20 mTorr; 200 W ICP.

ionization from $C_2F_4^+$ while CF_2^+ is only appreciably created through direct ionization from CF_2. The dominant neutral dissociated products are shown in Fig. 14. Electron impact reactions break apart c-C_4F_8 into primarily C_2F_4 [Fig. 14(a)] and CF_2 [Fig. 14(b)]. The density contours show them to also be distributed in an annulus, indicating that both species continue to be broken down after being formed. Otherwise, the peak density would be found in the center of the reactor, instead of being located near the point of maximum formation. At the center of the discharge, the c-C_4F_8 density (not shown) is about $4.0\times10^{14}\,\mathrm{cm}^{-3}$ giving a maximum dissociation fraction, for the present discharge conditions, of about 50%. Figure 15 shows the atomic Fluorine density contours. The present computations do not model polymer formation on the surfaces. The etching is, therefore, assumed to be in the limit of high ion bombardment. In this regime, the etch rate should be proportional to the atomic Fluorine concentration. The results indicate that, under the present conditions, the etch rate in the vicinity of the wafer chuck can be an order of magnitude larger than the etch rate on the reactor walls. This would be an important concern in the study or optimization of a chamber clean recipe.

Figure 16 shows the neutral temperature contours which result from solving the neutral energy equation. While most of the reactor is near 300 K, the discharge region has a peak temperature of about 1000 K. If the volume average temperature is calculated from the visible part of the reactor (underneath the coil housing), however, the indicated temperature is about 550 K, which is not very different from measurements (600 K) taken in similar experiments using C_2F_6.[8] Further work on the effects of neutral temperature on the plasma chemistry is in progress.

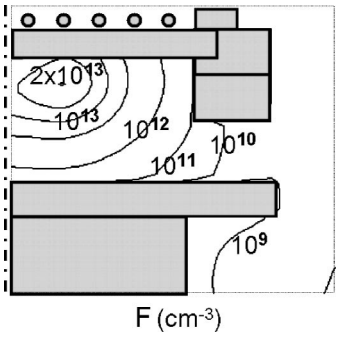

FIG. 15. Atomic Fluorine (F) density contours. Conditions: 10 sccm C_4F_8; 20 mTorr; 200 W ICP.

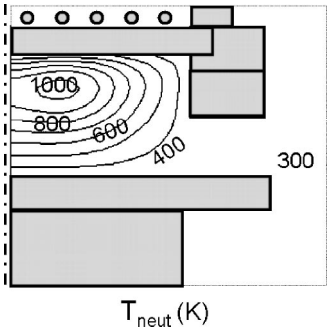

FIG. 16. Neutral temperature contours. Conditions: 10 sccm C_4F_8; 20 mTorr; 200 W ICP.

VI. SUMMARY

A numerical model for a c-C_4F_8 discharge has been constructed. A set of cross sections has been assembled for electron collisions with c-C_4F_8 based on a combination of *ab initio* calculations, beam measurements, and swarm (i.e., electron transport coefficient) analysis. We have proposed a neutral dissociation cross section and apparent attachment cross sections that give excellent agreement with a variety of measurements. In addition, a chemical reaction set has been proposed and a multidimensional numerical model has been used to test the cross section and chemical reaction set against experiments. Results show that measured trends are reproduced and absolute values are well represented. Several instances were identified where the macroscopic trend was not indicative of the microscopic details of the chemistry. For example, although the absolute amount of dissociation and F^- production is increasing with respect to pressure, the dissociation fractions and reaction rates are decreasing with increasing pressure.

ACKNOWLEDGMENTS

We would like to thank Dr. Zoran Lj. Petrovic for providing us with unpublished work of the late Professor Milan V. Kurepa. We would also like to thank Dr. Carl Winstead and Professor Vince McKoy for helpful discussions on electron collisions with c-C_4F_8 and for providing to us their unpublished work on CF_x radicals. This work has been supported in part by International Sematech, Inc.

[1] K. Sasaki, Y. Kawai, C. Suzuki, and K. Kadota, J. Appl. Phys. **83**, 7482 (1998).
[2] S. Samukawa, Jpn. J. Appl. Phys., Part 1 **33**, 2133 (1994).
[3] C. C. Allgood, S. Hsu, and M. Mocella, presented at the 199th Meeting of the Electrochemical Society, March 2001.
[4] C. C. Allgood, B. Birmingham, S. Hsu, and J. Soucy, International SEMATECH Tech. Transfer # 01024083A-TR, 2001.
[5] H. Hayashi, S. Morishita, T. Tatsumi, Y. Hikosaka, S. Kobayashi, S. Kimura, M. Inoue, T. Hoshino, and Y. Nishioka (private communication).
[6] C. Suzuki, K. Sasaki, and K. Kadota, Jpn. J. Appl. Phys., Part 1 **37**, 5763 (1998).
[7] A. N. Goyette, Y. Wang, M. Misakian, and J. K. Olthoff, J. Vac. Sci. **18**, 2785 (2000).
[8] G. A. Hebner, J. Appl. Phys. **89**, 900 (2001).
[9] G. A. Hebner, private communication, Sandia SEMATECH Report.
[10] D. Zhang and M. J. Kushner, J. Vac. Sci. Technol. A **19**, 524 (2001).
[11] K. Teii, M. Hori, T. Goto, and N. Ishii, J. Appl. Phys. **87**, 7185 (2000).

[12] H. Lee, H. Motomura, and K. Tachibana, Jpn. J. Appl. Phys., Part 1 **37**, 4522 (1998).
[13] Y. Chinzei, T. Ichiki, N. Ikegami, Y. Feurprier, H. Shindo, and Y. Horiike, J. Vac. Sci. Technol. B **16**, 1043 (1998).
[14] P. Ho, J. E. Johannes, R. J. Buss, and E. Meeks, Sandia Report SAND2001-1292, May 2001.
[15] H. Kazumi and K. Tago, Jpn. J. Appl. Phys., Part 1 **34**, 2125 (1995).
[16] W. L. Morgan, Adv. At., Mol., Opt. Phys. **43**, 155 (2000).
[17] J. P. Novak and M. F. Frechette, J. Appl. Phys. **63**, 2570 (1988).
[18] M. S. Naidu, A. N. Prasad, and J. D. Craggs, J. Phys. D **5**, 741 (1972).
[19] H. Itoh, T. Miyachi, M. Kawaguchi, Y. Nakao, and M. Tagashira, J. Phys. D **24**, 277 (1991).
[20] J. de Urquijo and E. Basurto, J. Phys. D **34**, 1352 (2001).
[21] M. Yamaji, Y. Okadam, and Y. Nakamura, in Proceedings of the International Symposium on Electron-Molecule Collisions and Swarms, Tokyo, 18–20 July 1999.
[22] C. Wen and J. M. Wetzer, IX International Conference on Gas Discharges and their Applications, Venezia, Italy, 19–23 September, 1988, p. 367.
[23] L. G. Christophorou and J. K. Olthoff, J. Phys. Chem. Ref. Data **30**, 449 (2001).
[24] C. Winstead and V. McKoy, J. Chem. Phys. **114**, 7407 (2001).
[25] J. E. Sanabia, G. D. Cooper, J. A. Tossell, and J. H. Moore, J. Chem. Phys. **108**, 389 (1998).
[26] H. Nishimura, in Proceedings of the International Symposium on Electron–Molecule Collisions and Swarms, Tokyo, 18–20 July 1999.
[27] C. Q. Jiao, A. Garscadden, and P. D. Haaland, Chem. Phys. Lett. **297**, 121 (1998).
[28] M. V. Kurepa, Trans. 3rd Czechoslovak Conf. On Electronics and Vacuum Physics, Prague, 1965; Z. Lt. Petrovic, private communication.
[29] S. M. Spyrou, S. R. Hunter, and L. G. Christophorou, J. Chem. Phys. **83**, 641 (1985).
[30] A. Chutjian and S. H. Alajajian, J. Phys. B **20**, 839 (1987).
[31] W. L. Morgan and B. M. Penetrante, Comput. Phys. Commun. **58**, 127 (1990).
[32] W. H. Press, S. A. Teukolsky, W. T. Vetterling, and B. P. Flannery, *Numerical Recipes in Fortran 77*, 2nd ed. (Cambridge University Press, New York, 1992).
[33] N. Gershenfeld, *The Nature of Mathematical Modeling* (Cambridge University Press, New York, 1999).
[34] W. L. Morgan, Phys. Rev. A **44**, 1677 (1991).
[35] W. L. Morgan, J. Phys. D **26**, 209 (1993).
[36] N. F. Lane, Rev. Mod. Phys. **52**, 29 (1980).
[37] W. L. Morgan, C. Winstead, and V. McKoy, J. Appl. Phys. **90**, 2009 (2001).
[38] K. Yoshida, S. Goto, H. Tagashira, C. Winstead, B. V. McKoy, and W. L. Morgan, J. Appl. Phys. (to be published).
[39] H. Toyoda, M. Iio, and H. Sugai, Jpn. J. Appl. Phys., Part 1 **36**, 3730 (1997).
[40] M. Radtke, J. W. Coburn, and D. B. Graves (in preparation).
[41] C. Winstead and V. McKoy, private communication.
[42] C. Winstead and V. McKoy, J. Chem. Phys. **114**, 7407 (2001).
[43] P. D. Haaland and C. Jiao, private communication.
[44] V. Tarnovsky, P. Kurunczi, D. Rogozhnikov, and K. Becker, Int. J. Mass Spectrom. Ion Processes **128**, 181 (1993).
[45] D. R. Bates and W. L. Morgan, J. Chem. Phys. **87**, 2611 (1987).
[46] W. L. Morgan and D. R. Bates, Astrophys. J. **314**, 817 (1987).
[47] A. P. Hickman, J. Chem. Phys. **70**, 4872 (1979).
[48] K. Dolden and B. Plant, Rep. Prog. Phys. **48**, 1283 (1985).
[49] R. A. Stewart, P. Vitello, and D. B. Graves, J. Vac. Sci. Technol. B **12**, 478 (1994).
[50] J. D. Bukowski, D. B. Graves, and P. A. Vitello, J. Appl. Phys. **80**, 2614 (1996).
[51] E. F. Jaeger, L. A. Berry, J. S. Tolliver, and D. B. Batchelor, Phys. Plasmas **2**, 2597 (1995).
[52] K. Waters, ''Infrared Diode Laser Absorption Spectroscopy Measurement of Gas Phase Radicals in C_4F_8 Discharges for Plasma Model Validation,'' Thesis, Chemical Engineering Dept. Univ. of New Mexico (2000).